6 STRAIN AND KINEMATIC ANALYSIS OF HIGH TEMPERATURE STRUCTURES

In chapter 4, I have shown that the deformational sequence can be subdivided into three main events, with an intermediate episode between D_1 and D_2, and a progressive passage from D_2 to D_3. The following sections will deal with a strain and kinematic analysis of the D_2 and D_{2-3} episodes. Although in some places strain determination of deformations predating D_2 is available, strain and kinematic analysis of such early structures have not been systematically performed due to the difficulty to correlate the observed mesostructures and deduced macrostructures with a general kinematic model.

The analysis of D_2 and D_{2-3} structures in areas where they formed under relative high temperature conditions is of special relevance for the purpose of understanding the relationships between three of interacting processes: deformation, metamorphism and magmatism. As far as the late D_3 event is concerned, its geometry and kinematics have been amply analysed in previous works, and only some global considerations will be made at the time of the discussion.

An approach to the tectonic setting at the time after D_2 deformation was given in section 4.3. (Fig. 38). In most of the area, a trend of heterogeneously developed sub-vertical foliations related to D_2 and also to D_{2-3} folding overprints previous N-S striking steep bedding and S_1 foliations. This fact entails the development of sub-vertical fold axes during D_2 and D_{2-3}. On the other hand, irrespective of these geometric relationships, stretching lineations are steeply dipping too (Fig. 83).

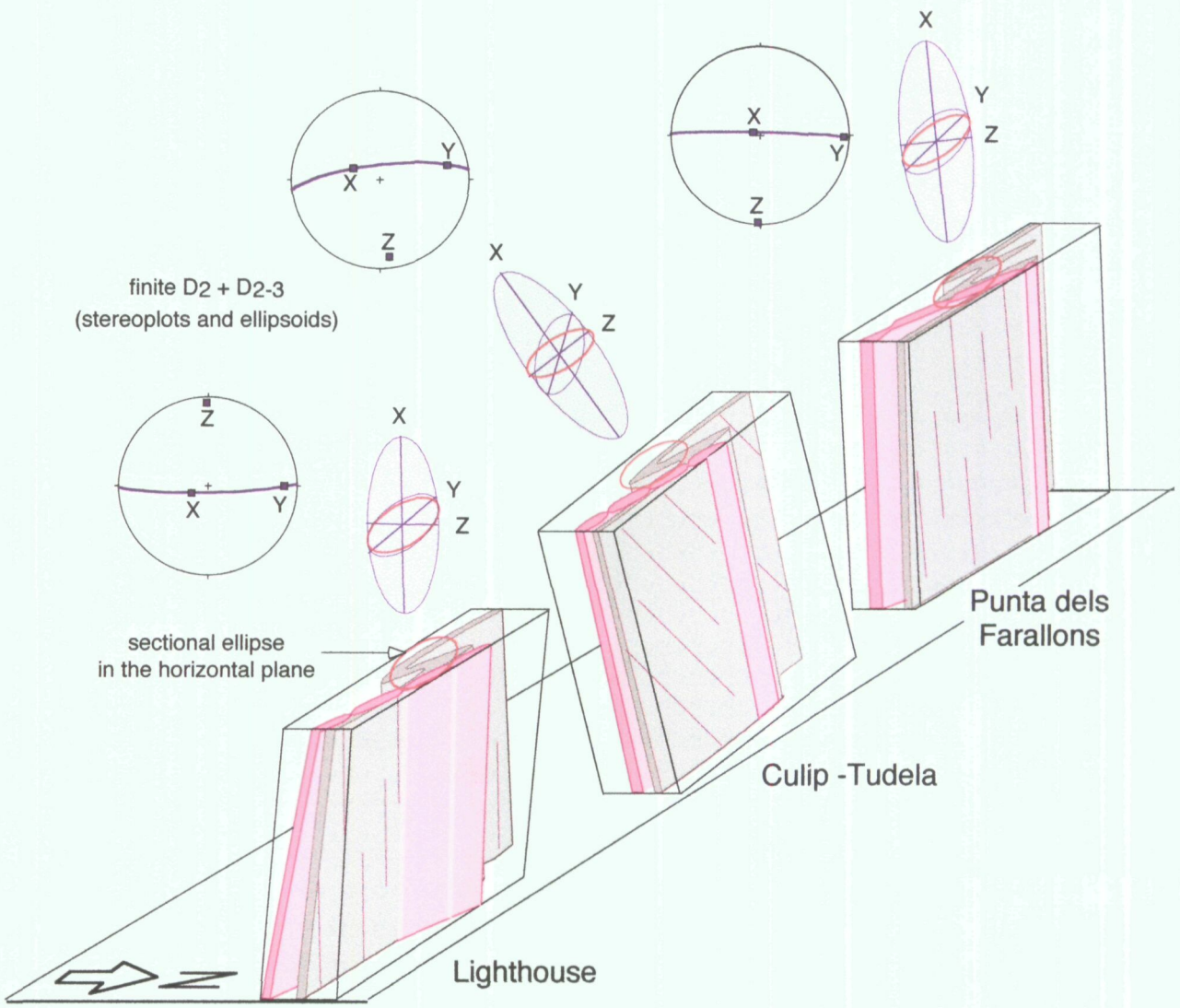

Fig. 83. Three-dimensional schematic representation of three medium to high D_2 to D_{2-3} strain selected subareas. The spatial orientation of the principal axes of finite strain are represented as qualitative ellipsoids and stereoplots.

Most features such folds, boudinage and asymmetric structures are better marked in flat-lying or gently dipping outcrop surfaces than in steep ones. The orientation of the X, Y and Z principal axes of the finite strain ellipsoid is given for three different medium to high strain subareas, accompanied by a qualitative sketch of the corresponding ellipsoids.

Small differences in the orientation in the principal strain axes in different subareas can in principle be attributed to inhomogeneous deformation along D_2 and D_{2-3} high strain zones and/or to late D_3-related rotations.

The intersection line between the previous anisotropy (S_1) and the flow plane (which lies close to the high strain zone boundaries) is subvertical and subparallel to the stretching direction.

The orientation of boudins in pegmatites may seem to contradict the idea that subvertical extension is important. Some of the steeply dipping pegmatites show boudinage in a vertical direction, but boudins with steep axes subparallel to the stretching lineation seem dominant in all low to high strain domains. Boudin necks do not show any evidence of having undergone rotation. In most outcrops, however, the location of boudin necks can be seen to coincide with the intersection line between the pegmatite wall and the subvertical $S_{S/1}$ foliation. It follows the possibility of boudin axes developing parallel to this intersection. Talbot (1970) and Karlstrom & Williams (1995) described similar settings where boudin necks lie at a low angle from the longest axis of the strain ellipsoid. On the other hand, if pegmatites undergone some extension parallel to Y axis, it follows that flow type deviated from plane strain to flattening strain.

The first step in the reconstruction of the geometry and kinematics of the area will be to proceed with a two-dimensional analysis of the structures observed in sub-horizontal sections, taking into account that these sections are subparallel to the ZY plane and normal or highly oblique to the stretching lineation and hence to the X axis of the finite strain ellipsoid.

6.1. ANALYSIS IN HORIZONTAL SECTIONS

Strain and kinematic analysis in horizontal sections has been mainly performed in the Culip-Cap de Creus area. Several reasons make this selected area appropriate for such studies. First, the continuous exposure conditions; second, the simplicity of the structures if comparing with other nearby areas and the presence of sets of differently oriented quartz veins and pegmatite dykes; and third, although strain is rather inhomogeneously distributed over the area, strain gradients are well controlled, and structural domains with relatively high and low strain can be distinguished. Some other areas surrounding the Punta dels Farallons zone are also adequate to such studies, and data have also been collected from there. However, most structures are strongly transposed in this latter zone due to high strains, inhibiting their use in strain analysis.

6.1.1. DEXTRAL DEFLECTION: FIRST APPROACH

The main features of the structure of the Culip-Cap de Creus area have been profusely described in sections 4.4.1. and 5.3.1. As a reminder, the change in orientation of both S_1 foliation and S_2 crenulation cleavage from the low strain into the high strain zone defines a cylindrical sigmoidal structure associated to a dextral flexure in map view. Assuming that the fan-like pattern of the crenulation cleavage trajectories in rocks with low mechanical anisotropy should track approximately the XY plane of finite strain, it follows that there is a non-coaxial component to the deformation. The fact that, as a result of deformation increase, the trace of the XY plane rotates dextrally about a sub-vertical axis, suggests that on the regional scale, a dextral shear component may have been involved. The general structure could be interpreted as a large dextral simple shear zone. However, dextral simple shearing is not congruent with the 60° rotation of the XY finite deformation plane from lower strain domains (where crenulation cleavages trend N30) to higher strain domains (where crenulation cleavages trend N90). The maximum rotation allowed by heterogeneous simple shear is of 45° (Fig. 84, top). Moreover, strains recorded in

the lower strain domains would correspond for simple shear to a foliation making less than 30° with the flow plane. In these low strain domains, an average strain ratio R=2 has been determined from deformed early quartz veins (Fig. 85).

A model considering shear plus shortening (Fig. 84, bottom), which bear analogies with the domains of inhomogeneous coaxial shortening in the model of Bell (1981), would explain satisfactorily the large stretches recorded in the low strain domains but, on the contrary, it would limit the rotation of the XY plane of the finite strain ellipsoid to less than 45°. The large rotation excludes therefore any model considering bulk heterogeneous closely coaxial deformation. Analysis of minor structures will provide additional evidences in order to unravel the general structural pattern.

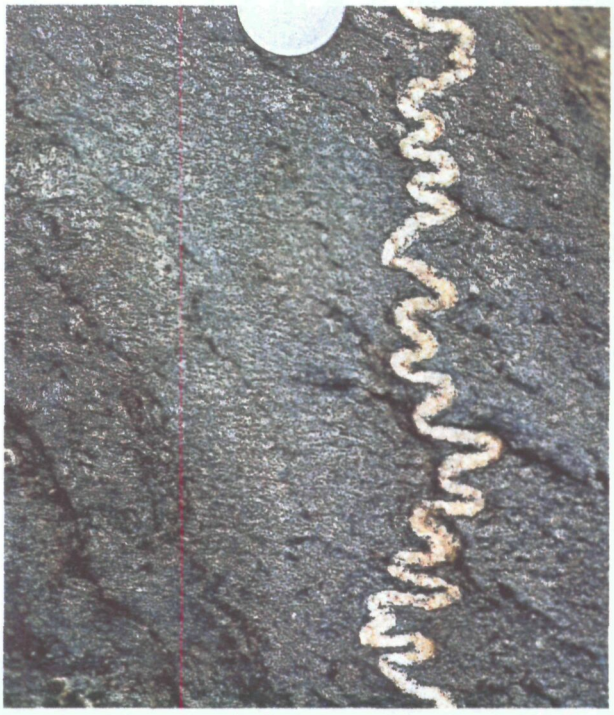

Fig. 85. Horizontal view of a folded quartz vein, used to measure stretch in low strain domains (Puig de Culip).

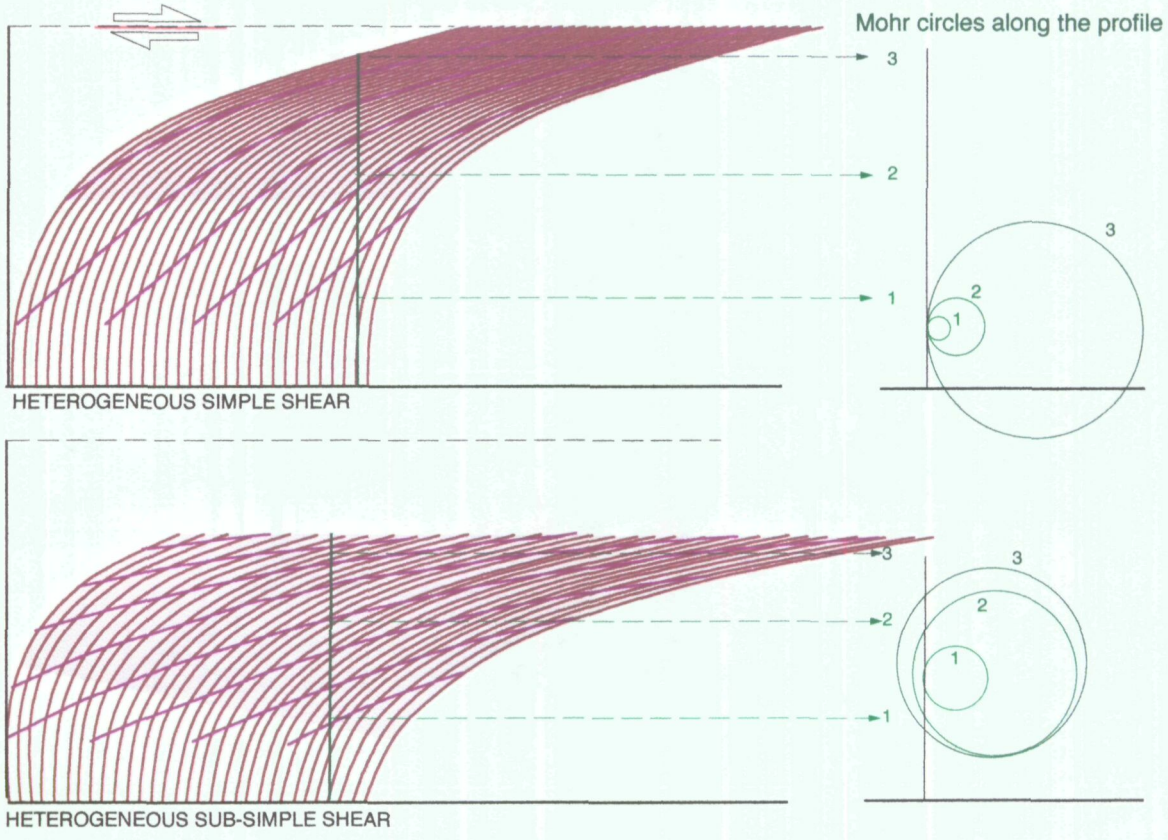

Fig. 84. Schematic approaches to explain the dextral deflection observed in horizontal sections and, thus, the rotation of both S_1 (in brown) and S_2 (in violet) foliations. Both models are based in heterogeneous progressive deformation and differ in flow type: simple shear (top) and sub-simple shear (bottom). Shaded areas in violet represent domains of higher strain. Mohr circles for strain have also been drawn for different deformation gradients along a profile perpendicular to the flow plane.

6.1.2. KINEMATIC INDICATORS

Several small scale asymmetric structures in horizontal planes are indicative of shear sense of flow (e.g. geometry of quartz vein structures and inclusion patterns in porphyroblasts). All these structures show the prevalence of a sinistral layer-parallel shearing throughout the zone, which is in principle in manifest contradiction with the dextral flexure described above.

Porphyroblast rotation

Porphyroblasts of andalusite up to 5 cm in diameter occur all over the study area (Fig. 86a). The S_1 foliation is deflected around these andalusites but is continuous with a straight inclusion pattern Si. Most porphyroblasts show anti-clockwise rotation with respect to Se. Variable amounts of sinistral rotation from 0° to 100° are recorded.

Sigmoidal quartz-rods

The pre-D_2 quartz veins usually display D_2 boudinage or folding structures depending on their original orientation. Those which were boudinaged before the onset of D_2, develop into a peculiar shape during D_2 as a result of general shortening of the veins and anti-clockwise rotation of the boudins with respect to the S_1 foliation by progressive D_2 to D_{2-3} deformation.

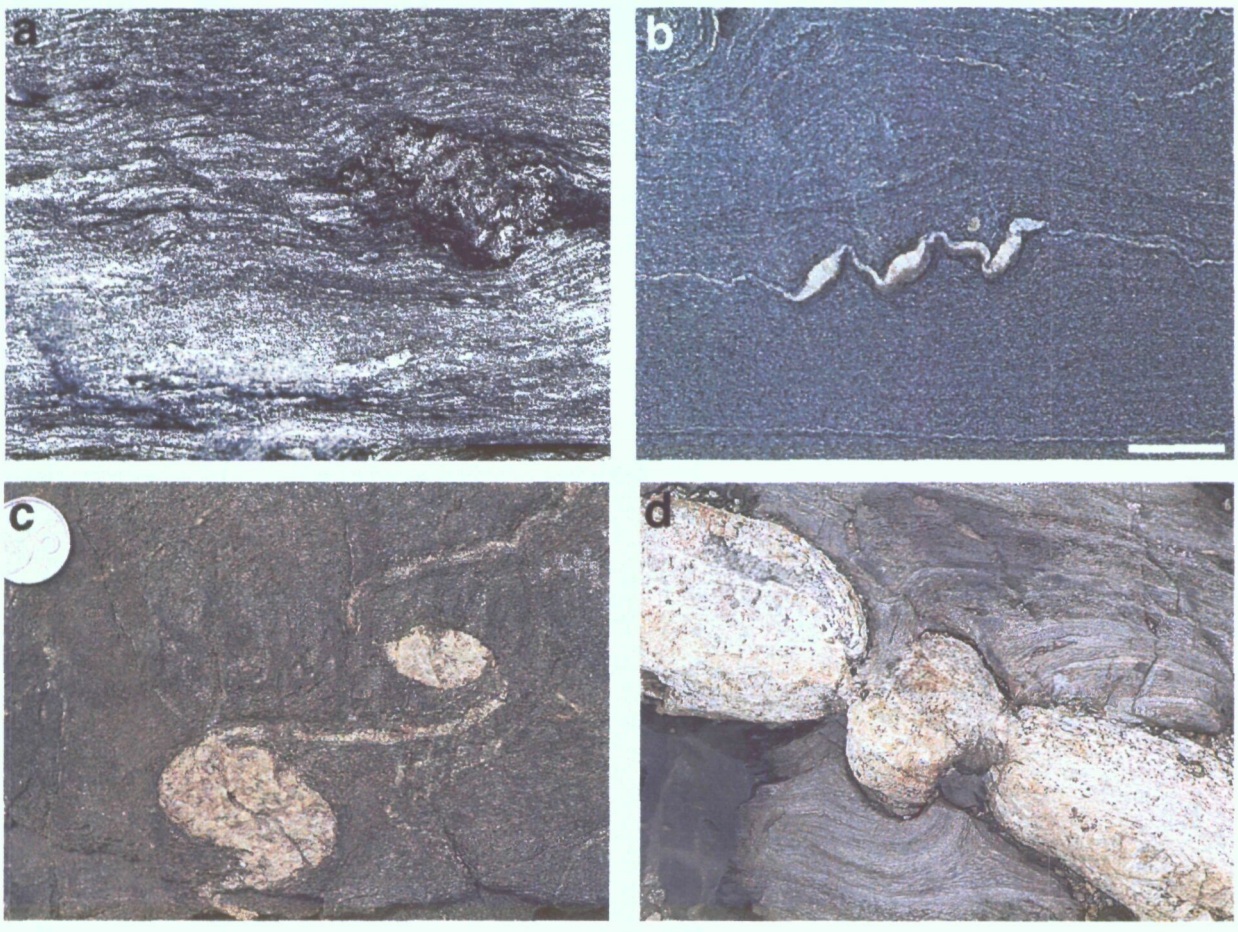

Fig. 86. Field photographs of small scale kinematic indicators (sub-horizontal views). (a): Andalusite porphyroblast sinistrally rotated with respect to the S_1 foliation. Scale bar = 2 cm (south Cala Cullaró). (b): Sigmoidal quartz-rod structure resulting from folding and rotation of early boudinaged quartz veins (see text for explanation). The widest part of the boudins are located in the short limbs of the folds. Scale bar = 2 cm (Puig de Culip). (c): Other sigmoidal quartz-rod structures (lighthouse zone). In this case, the quartz vein structure resembles d-shaped mantled porphyroclasts. (d): Boudinaged pegmatite dyke (lighthouse zone). A short boudin is sinistrally rotated with respect to the pegmatite vein enveloping surface, inducing a complex folding pattern in the enclosing metasediments. Width of view 80 cm.

These structures, designed as sigmoidal quartz-rods (Druguet et al. in press), develop an asymmetric shape on horizontal surfaces with the widest part of the boudins systematically located in the short limbs of the folds (Fig.86b). The angle of obliquity between these quartz- veins and the S_1 plane varies from 0° to 170° (in an anti-clockwise sense). Short, stocky boudins develop a shape resembling d-shaped mantled porphyroclasts (Fig.86c). Where a crenulation cleavage is present, its orientation in the embayments of the quartz vein structures makes a larger angle with S_1 than in the wall rock, suggesting lower strain in these domains (Fig. 40, chapter 4). S_1 is usually straight in the wall rock and wraps around the sigmoidal quartz-rods. Throughout the area, in high and low strain zones, sigmoidal quartz-rods have an S-geometry on horizontal pavements. In three dimensions, the structures are highly cylindrical with the symmetry axis parallel to the stretching or intersection lineations. There are some decametric-scale folds where both limbs contain 10 cm-sized quartz rods with identical vergence despite the limb change, showing that folding locally postdated the development of sigmoidal quartz-rods, which are not simply small scale D_2 folds.

The geometry of the sigmoidal quartz-rods indicates that they formed by relative rotation of the massive D_1-boudins by variable angles with respect to $S_{S/1}$ foliation. The massive boudins in quartz veins would had acted as relatively competent bodies during D_2 flow.

Pegmatite boudins

Some pegmatite boudins show reorientation of their long axes indicating anti-clockwise rotation of the boudin with respect to the pegmatite vein enveloping surface. Such asymmetric structures develop preferentially in short pegmatite boudins (Fig . 86d), in a similar way as the porphyroblasts and quartz-rods. Possibly, after the emplacement of pegmatite dykes, boudinage was followed by rigid body rotation of the shortest boudins.

Other interesting structures have been observed in a 20 m wide pegmatite dyke from the Punta dels Farallons migmatite complex (Fig. 68a, chapter 5). The dyke is trending E-W, in close parallelism with the transposition foliation in the enclosing schists, and shows NE-SW-trending spaced foliation bands across its walls which resemble an initial stage of asymmetric boudinage. A high temperature solid state fabric is developed along the bands within the pegmatite. The observed asymmetry indicates once more a sinistral sense of shear operating in the horizontal plane.

6.1.3. SECOND APPROACH

The following two-dimensional models are proposed to reconcile (i) the dextral deflection pattern affecting both bedding-S_1 foliation and the crenulation cleavage and (ii) the foliation-parallel sinistral shearing inferred from small scale kinematic indicators. In Fig. 87 (top), bedding-S_1-parallel shear is considered one of the main mechanisms involved during deformation. Sinistral bedding and S_1 parallel shearing and flexural folding enables the clockwise rotation of these structures resulting in a bulk dextral super-simple shear, while schists accommodate the bulk deformation by internal sinistral flow. The bulk dextral flexure-induced rotation is greater than the S_1 parallel anti-clockwise flow, in a similar way as occurs in a flexural flow fold (Ramsay 1967). This fact explains the overall dextral rotation of S_1 and S_2. However, the flexural flow model does not explain the layer-parallel shortening and associated large stretches recorded in the low strain domains. To compatibilize this, a component of homogeneous sub-simple shear have been added to the flexural flow model (Fig. 87, bottom). In analogy to parasitic folds (De Sitter 1958) developed in larger structures, minor folds would nucleate as a result of contractional strain along the $S_{S/1}$ foliation, possibly anticipating the development of the larger sized structure. The resulting model is consistent with all observations (Fig. 88) and, moreover, with strain and vorticity determinations obtained from deformed quartz and pegmatite dykes (next section). However, the limitations of these models must be considered, since they represent simplified approaches which do not account for, for instance, the evident area change in the analysed plane.

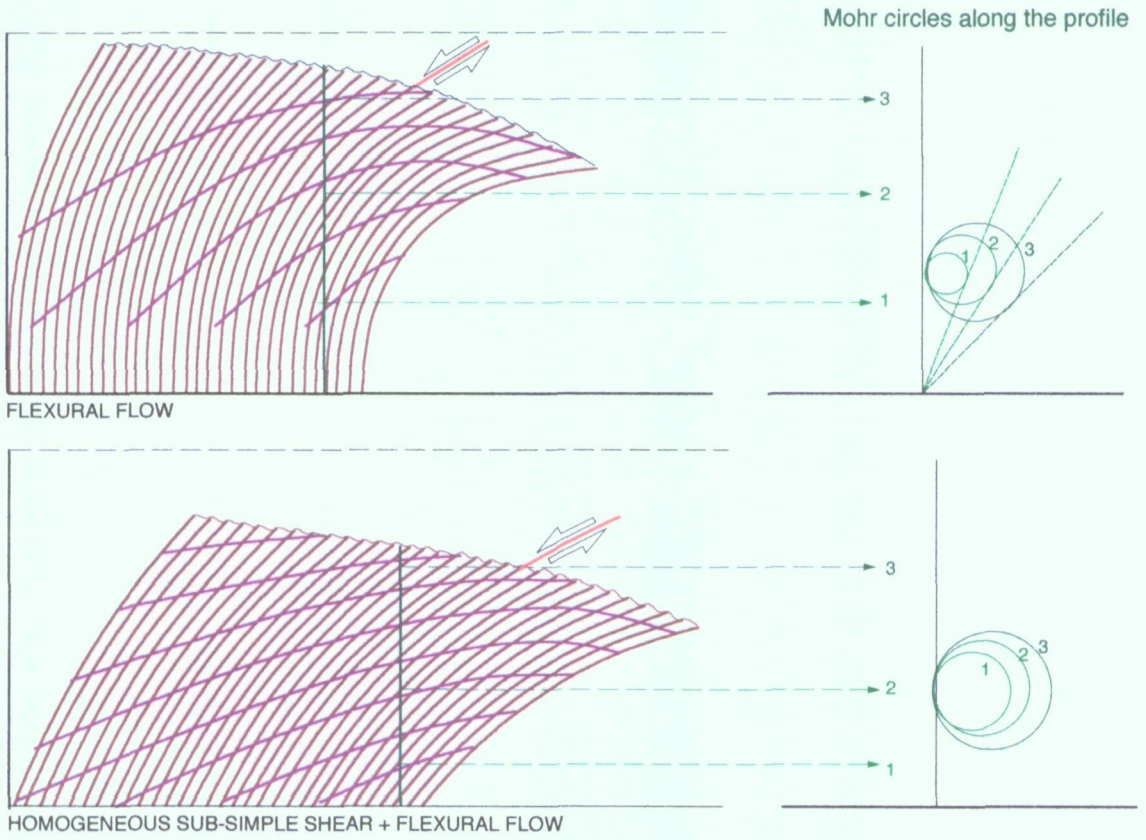

Fig. 87. Schematic models to explain the dextral deflection and the S1-parallel sinistral shearing, both observed in horizontal sections. See Fig. 84 for legend. Both models are based in heterogeneous progressive deformation and differ in flow type: flexural flow (top) and homogeneous sub-simple shear plus flexural flow (bottom). Dashed lines in the top Mohr diagrams represent reference axes if we consider the S1 foliation as the flow plane. In this case, the obtained Mohr diagrams indicate sinistral shearing.

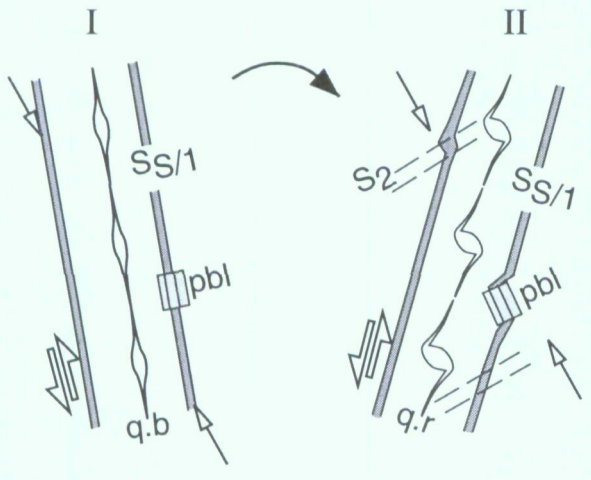

Fig. 88. Idealized sketch showing the evolution of some geometrical and kinematical elements involved in the development of high temperature structures. I: initial stage; II: after some deformation involving bulk dextral rotation, S1-parallel sinistral non coaxial flow and oblique shortening. pbl: porphyroblast; q.b: quartz boudins; q.r: quartz rods. (Modified after Druguet et al. 1997).

6.1.4. STRAIN DETERMINATION

Procedure for the case study

Two dimensional strain will be graphically represented either in physical space, using the strain ellipse, and in Mohr space, using the Mohr construction for finite strain (Means 1982, De Paor & Simpson 1993, Fig. 89). In the Mohr construction for strain the polar coordinates of a point on the circle represent the stretch S and rotation α of a certain line. The polar reference axis is normal to a non-rotating line, such as the flow plane. If deformation is irrotational, the Mohr circle is centered on the polar reference axis, otherwise the circle's central axis is oblique to the reference axis. The points on the circle that are farthest from and nearest to the origin represent the lines of maximum and minimum stretch: S_1 and S_2. They were initially orthogonal in geographical space and, having undergone equal rotations (ω), they are also orthogonal after deformation, and represent lines of no shear strain.

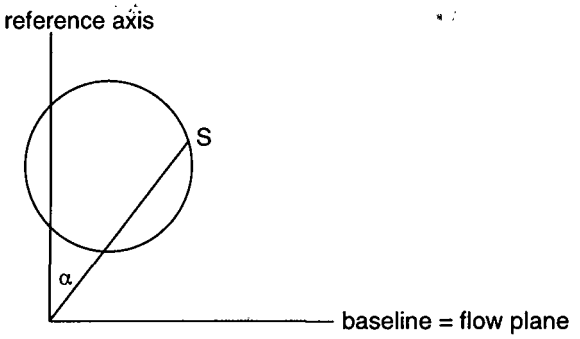

Mohr construction for strain employing polar coordinates of longitudinal strain (stretch, S) and angular strain (rotation, α)

ξ_1 and ξ_2 : lines of no rotation (eigenvectors)

Infls : lines of no finite longitudinal strain, separating shortening and extending fields

S_1 and S_2 : principal finite stretches

Wk = cos (ξ_1 ^ ξ_2) : kinematic vorticity number

Wk = 0 coaxial deformation
Wk ≠ 0 non-coaxial deformation

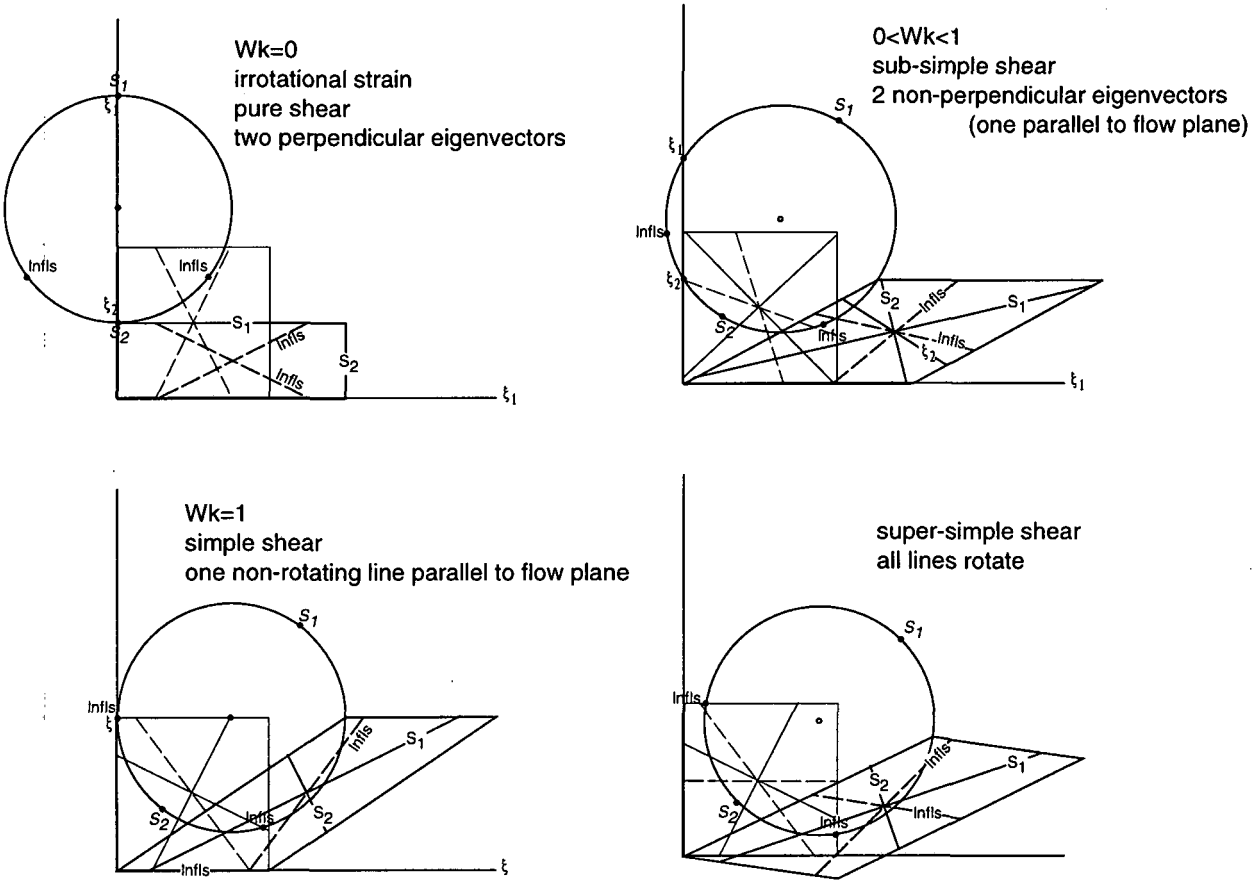

Fig. 89. Mohr construction for two-dimensional strain and representation of four main types of shear deformation as Mohr circles and deformed squares. No area change and an axial ratio R=4 have been considered for the four examples. Nomenclature after De Paor & Simpson (1993).

The points intersecting the reference axis represent lines of no rotation and are called eigenvectors or flow apophyses. The initial and final geographic orientations of each line can be obtained from its corresponding point in the Mohr space so that a pair of undeformed and deformed cells can be drawn.

Sets of differently oriented quartz veins and pegmatite dykes have been used as strain markers to determine the stretch values and the related best fit finite strain ellipse, following standard strain analysis techniques (e.g. Talbot 1970, Hutton 1982, Ramsay & Huber 1983, Passchier 1990, Talbot & Sokoutis 1995). Each individual outcrop selected for analysis shows a rather homogeneous deformation, with constant orientations of S_1, S_2 and S_{2-3} foliations. While the early quartz veins record the bulk deformation, the pegmatite sets record only part of deformation, i.e. at post-dating their emplacement. Bulk strain determinations have not been performed in higher strain domains, because the transposition of all earlier structures into a closely parallel trend prevents their use in strain analysis. From these ellipses, the area change and the local strain ratio (R) can be determined. They are sectional ellipse values and consequently represent lower values than those corresponding to the X/Z ratio of the strain ellipsoid expected to lie in subvertical planes.

The principal finite stretches give the diameter of the Mohr circle and its distance to the origin. Determination of the position of the Mohr circle in regard to the reference axis needs absolute rotation values and these values are determined after making some assumptions: (i) in the lowest strain domains, the S_1 foliation has an average N170 trend; (ii) clockwise rotation of the S_1 foliation about a vertical axis during D_2 and D_{2-3} deformation is considered (from N170 to its present disposition) as a result of non coaxial flow. Geographic coordinates are used as reference frame; (iii) some clockwise rotation of S_1 had already occurred before the emplacement of pegmatite dykes in medium to high strain domains. The eigenvectors have been determined following these assumptions, and hence the vorticity of the flow and the initial orientation of linear elements (veins) in a geographic horizontal surface.

Bulk strains recorded by early quartz veins

Strain analyses from early quartz veins has been performed only in two localities corresponding to low strain domains (Fig. 90 and Fig. 91). Strain ratio values obtained from the ellipses confirm the observed large stretches even in the locality with lowest strains (Puig de Culip 1). An area loss of 37% in average has been also found. This area loss in the horizontal plane is consistent with the apparent strong extension in a vertical direction, if volume is to be conserved. Because area decreasing in this section, the field in the finite strain ellipse where veins have been shortened is larger than that where they have been extended. This explains why most measurable quartz veins have been folded or folded plus boudinaged. Even the $S_{S/1}$ foliation (which would be expected to undergo extension if no area change), appears slightly shortened, also in consistency with the observed open folds in these low strain domains. Mohr diagrams reveal that sub-simple shear was prevalent, although in the lowest strain locality the determined vorticity is lower, deviating to a more coaxial flow.

Strain recorded by pegmatite dykes and related quartz veins

Strain analysis from pegmatite dykes has been performed for three localities in the Culip-Cap de Creus medium strain domains (Fig. 92, Fig. 93 and Fig. 94) and for another in the Punta dels Farallons (Fig. 95). In the Sa Claveguera outcrops (Fig. 96), some synkinematic quartz veins, genetically related to pegmatites, have been used for the analysis.

The strains recorded by these dykes are assumed to represent finite strains during D_{2-3}, since their synkinematic character with respect to progressive D_2 to D_{2-3} deformation.

An average strain ratio R=3 is recorded in dykes from medium strain domains. The corresponding total strains in these medium strain domains are expected to be larger, as indicated by the difference in tightness of coaxially folded schists and pegmatites and by comparison with the large strain values recorded in schists from low strain domains.

Area change in these domains is minimal or even positive (area increase of about 20% in the locality "Sa Claveguera"). Assuming that: (i) the bulk

deformation in the area involved an area decrease of at least 30% in the horizontal sections and (ii) pegmatites in the medium strain domain occupy at most 15% of the overall horizontal surface, it follows that this 15% increasing area may balance the tectonic 30% decrease, leaving a total 15% area decrease. The achieved area-increasing values might be explained by local volume increase.

Mohr diagrams reveal that sub-simple shear was prevalent during D_{2-3} deformation, with an average value of Wk=0.8. The determined flow implies dextral rotation of the S_1 foliation of up to 60° during D_{2-3}. Dykes emplaced sub-parallel to S_1 would rotate more or less the same, whereas other dykes are shortened or extended, and rotate dextrally or sinistrally, depending on their original orientation. However, in such sub-simple shear, there is an small field where dykes are able to rotate sinistrally and, in these cases, they record short amounts of rotation till they are blocked by the extensional eigenvector, which would act in this case as a "fabric attractor" in the sense of Passchier and Trouw (1996) and Passchier (1997).

The bulk sub-simple shear, however, is achieved by S_1 parallel sinistral shearing, and that can be noticed if the geographical external reference frame is substituted by S_1 foliation (see Mohr diagram in Fig. 93 and Fig. 87). The linear elements of all veins rotate sinistrally with respect to S_1 foliation.

Another significant result is the obliquity of the long axis of the measured ellipses with the orientation of the crenulation foliation and the long axis of the bulk strain ellipses (Fig. 90). This fact evidences the non-coaxiality of the deformation, being the bulk strain ellipse sinistrally rotated with regard to the strain ellipse recorded by the pegmatite dykes.

The small change in orientation experienced by the dykes from the intrusion to their present attitude (especially the approximately E-W-trending, prevalent ones) enables to conclude that many pegmatites were injected in close parallelism with the traces of the crenulation foliation and with the axial traces of D_2 to D_{2-3} folds.

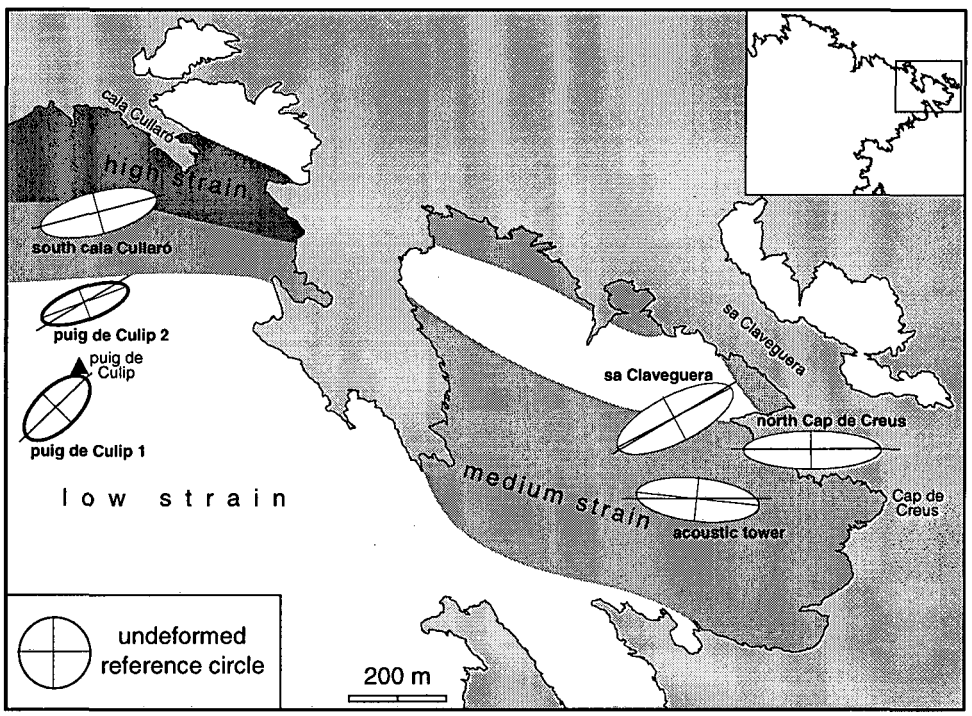

Fig. 90. Schematic map of the Culip-Cap de Creus area, showing the arrangement of different structural domains and sectional strain ellipses. Thick ellipses represent bulk D_2 + D_{2-3} strains recorded by early quartz veins. Thin ellipses represent strains recorded by pegmatites. The short and long axes of different ellipses are drawn, as well as the mean orientation of the crenulation cleavage.

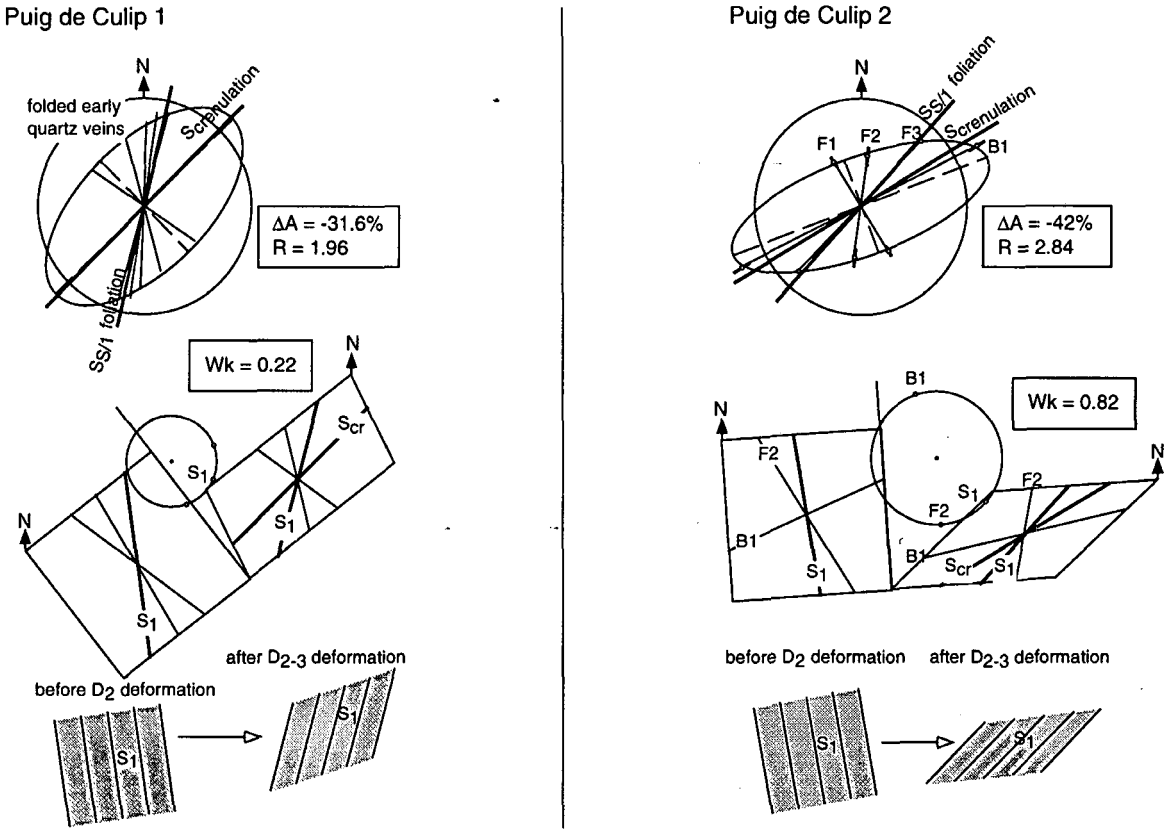

Figs. 91. Strain and kinematic analysis of D2 + D2-3 structures in low strain domains. The sectional ellipses, Mohr diagrams and the set of undeformed and deformed cells have been constructed using the method explained in page 122. Bulk D2 + D2-3 strains are recorded by early quartz veins. F: folded quartz veins, B: boudinaged. The location of the analysed areas are indicated in Fig. 90.

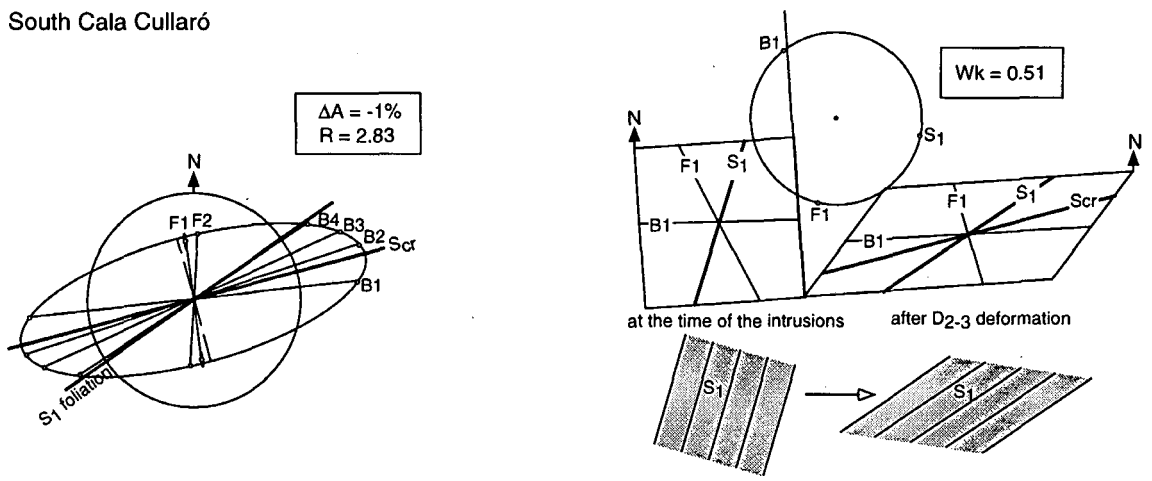

Figs. 92. Strain and kinematic analysis of D2-3 structures in a medium strain domain. The sectional ellipse, Mohr diagram and the set of undeformed and deformed cells have been constructed using the method explained in page 122. D2-3 strains are recorded by syntectonic pegmatite dykes. F: folded pegmatites, B: boudinaged. The location of the analysed area is indicated in Fig. 90.

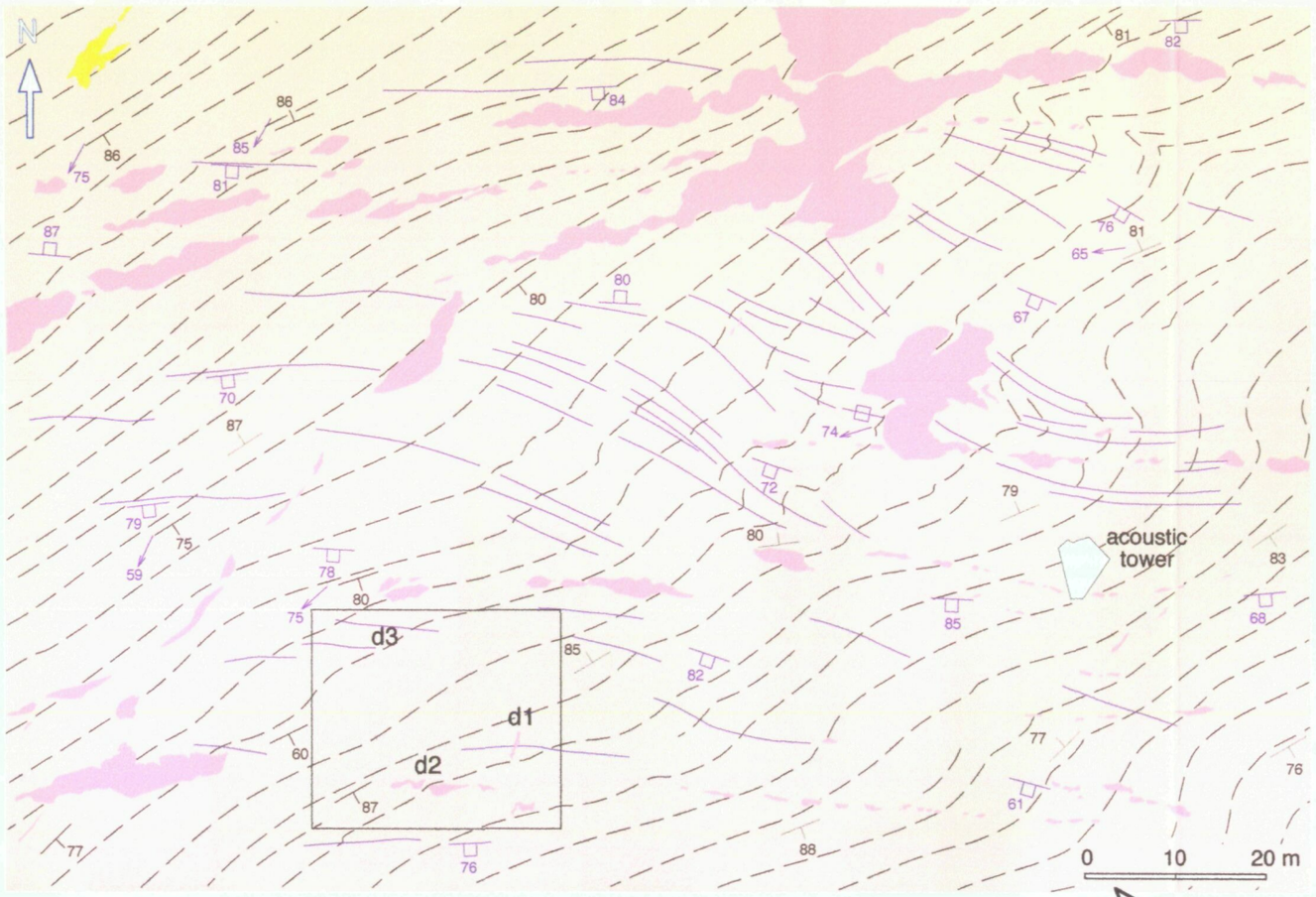

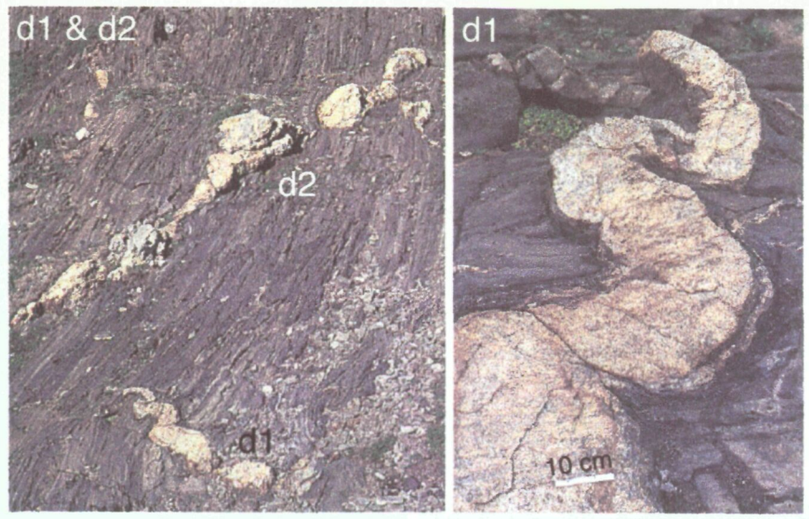

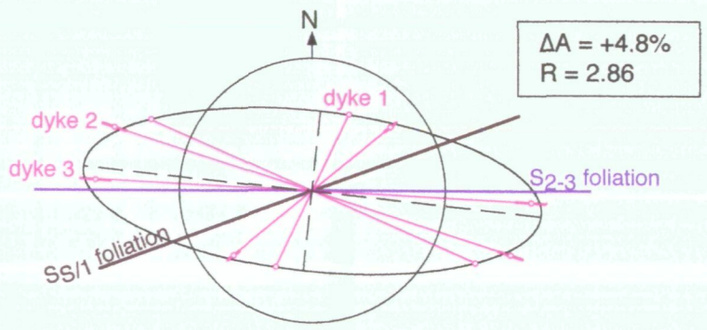

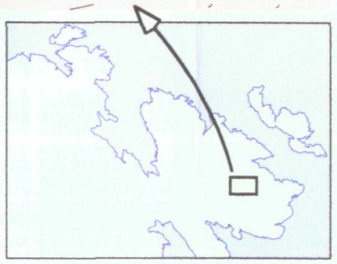

quartz veins

pegmatites

metagreywackes and metapelites

S_2 to S_{2-3} foliations and L_2 to L_{2-3} lineations (progressive deformation)

bedding-S_1 foliation

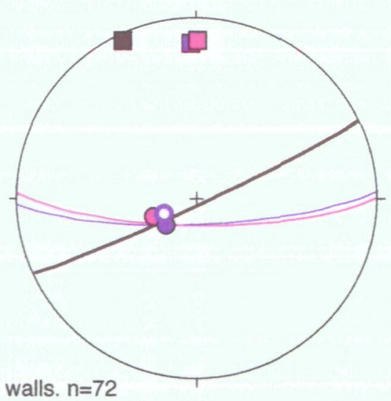

mean poles to surfaces

- pegmatite walls. n=72
- $S_2 + S_{2-3}$ crenulation foliation. n=71
- S_1 early foliation. n=102

same colors for mean values of foliations

- pegmatite boudin necks, mean vector. n=9
- $L_2 + L_{2-3}$ stretching lineation, mean vector. n=11
- $L_2 + L_{2-3}$ fold axis, mean vector. n=29

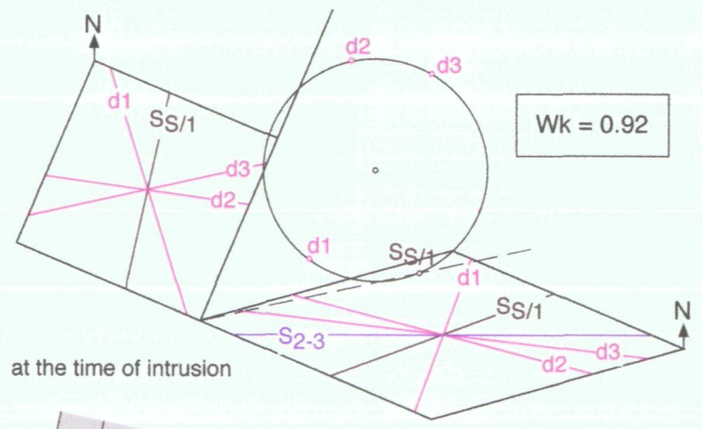

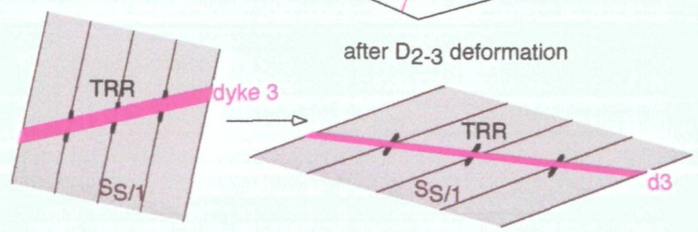

Fig. 93. Detail structural map of the acoustic tower zone with equal area lower hemisphere projections of main structural elements. Strain and kinematic analysis of deformed pegmatite dykes. The analysed area is represented by a square in the map. d1, d2 and d3: dykes; TRR: Tourmaline rich rim.

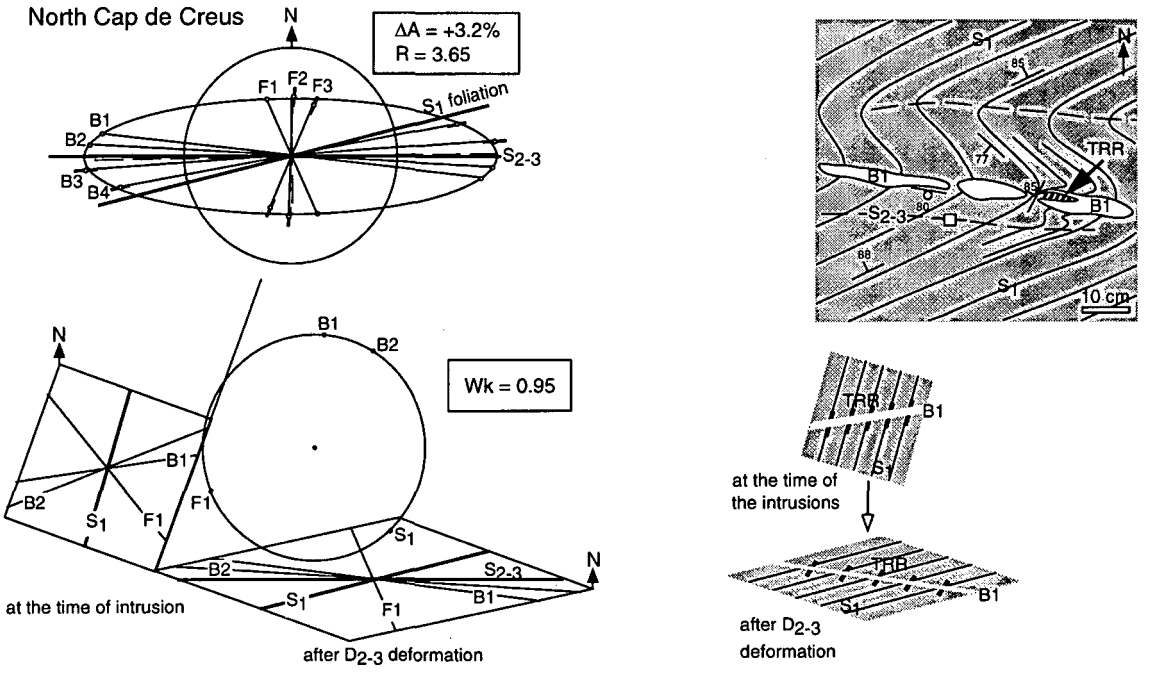

Figs. 94. Strain and kinematic analysis of D2-3 structures in a medium strain domain. The sectional ellipse, Mohr diagram and the set of undeformed and deformed cells have been constructed using the method explained in page 122. D2-3 strains are recorded by syntectonic pegmatite dykes. F: folded pegmatites, B: boudinaged pegmatites, TRR: tourmaline rich rim. The location of the analysed area is indicated in Fig. 90.

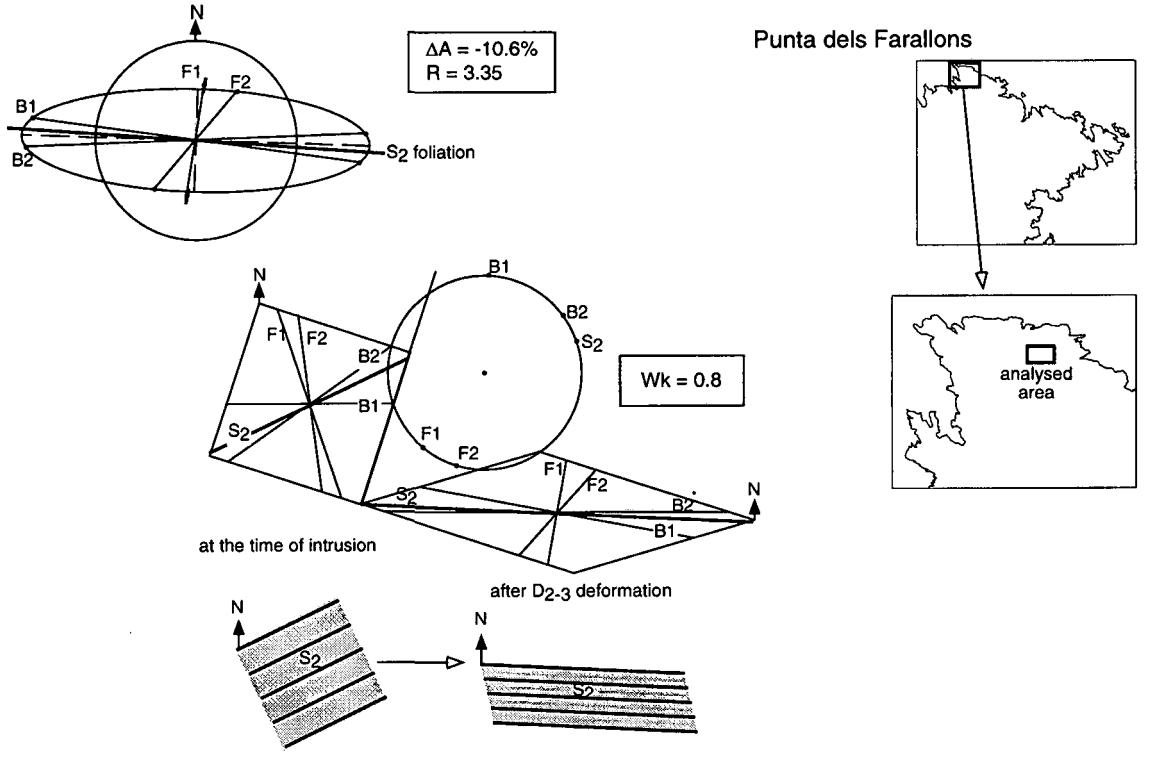

Fig. 95: Two-dimensional strain and kinematic analysis of syntectonically deformed pegmatite veins and dykes from the Punta dels Farallons migmatite complex. The sectional ellipse, Mohr diagram and the set of undeformed and deformed cells have been constructed using the method explained in page 122. In this case, a 30° dextral rotation of the S2 foliation due to D2-3 strain has been assumed by comparing the orientation of the S2 foliation in this area with its orientation in southern zones of low D2-3 strain. F: folded pegmatites, B: boudinaged pegmatites.

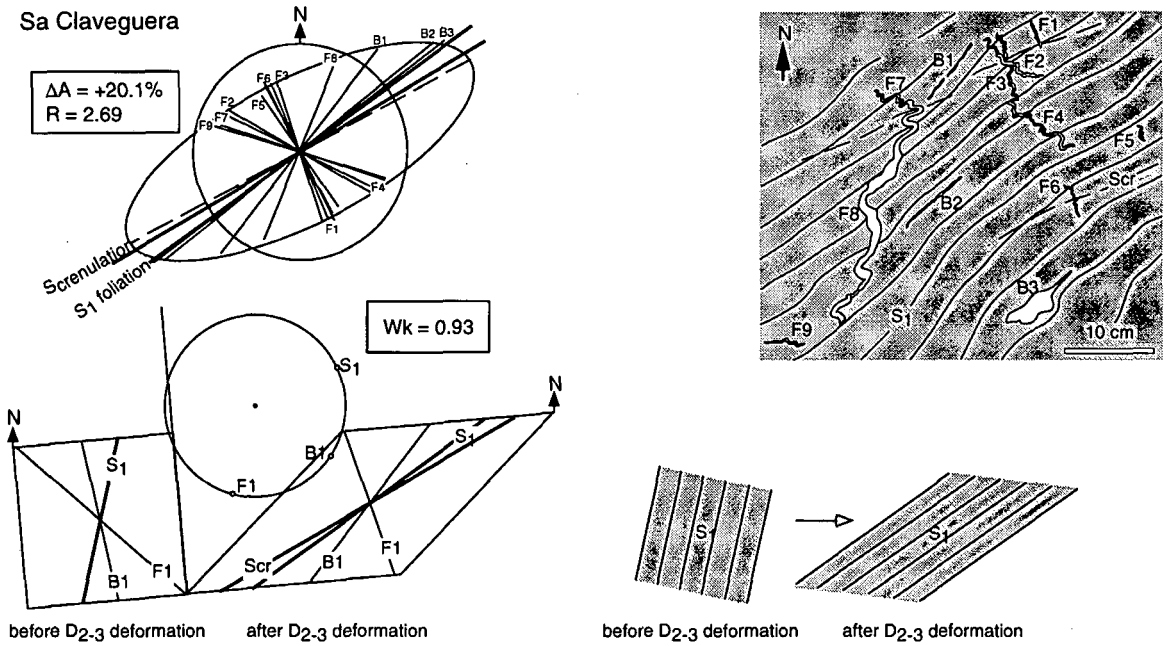

Figs. 96. Strain and kinematic analysis of D2-3 structures in a medium strain domain. The sectional ellipse, Mohr diagram and the set of undeformed and deformed cells have been constructed using the method explained in page 122. D2-3 strains are recorded by syntectonic quartz veins. F: folded pegmatites, B: boudinaged pegmatite. The location of the analysed area is indicated in Fig. 90.

Inferences from tourmaline-rich rim structures

The tourmaline rich rim (TRR) structures, introduced in section 5.3.1., have been considered as indicators of the initial angle between $S_{S/1}$ and the pegmatite dykes when these intruded. Actually, the angular relationships between S_1 foliation and pegmatite walls at the time of intrusion are sealed to the dykes at their TRR due to tourmalinization. Thus the bulk rotation angle is:

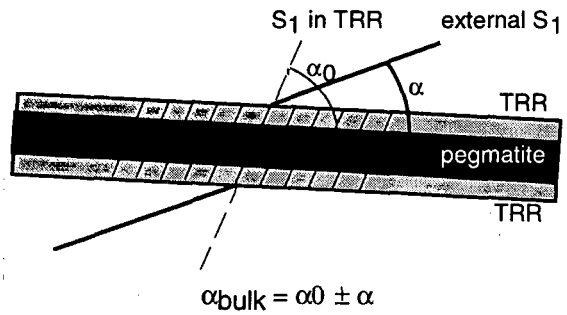

$$\alpha_{bulk} = \alpha 0 \pm \alpha$$

(- if both the S_1 foliation and the pegmatite rotate in the same sense and + if they rotate in opposite sense)

where α_0 is the angle between S_1 preserved in the TRR and the pegmatite wall, and α is the angle between the external S_1 and the pegmatite wall.

In most of the places where these structures have been observed, the ghost foliation sealed to the TRR is commonly oblique to $S_{S/1}$ further away in the wall rock, indicating relative rotation of dykes with their TRR and S_1 in the wall rock. After restoration of deformation, it appears that while in the location "North Cap de Creus" (Fig. 94) the orientation of different elements in the resulting deformed cell is consistent with the angle between the pegmatite wall and the S_1 preserved in the TRR, in the "acoustic tower" location (Fig. 93), the angular relation obtained in the deformed cell does not coincide with the observed one. In this latter outcrop (see photograph corresponding to dyke 3), the angle between the dyke and the S_1 foliation preserved in the TRR is higher than in the deformed cell. Since only the long limbs of minor folds (in close parallelism with the enveloping surfaces) have been plotted in the diagrams, it follows that the pegmatite in this case was emplaced across the short limb of a pre-existing minor F_2 fold. These relationships are schematically interpreted in Fig. 97. Inferences from these structures are consistent with (i) the assumed syntectonic character of dykes in regard to progressive deformation, and (ii) the fact that F_2 folds might control the intrusion of E-W dykes. In Fig. 98 there is an example of a small pegmatite vein intruding parallel to the axial plane of a "S" minor fold, while developing a TRR structure.

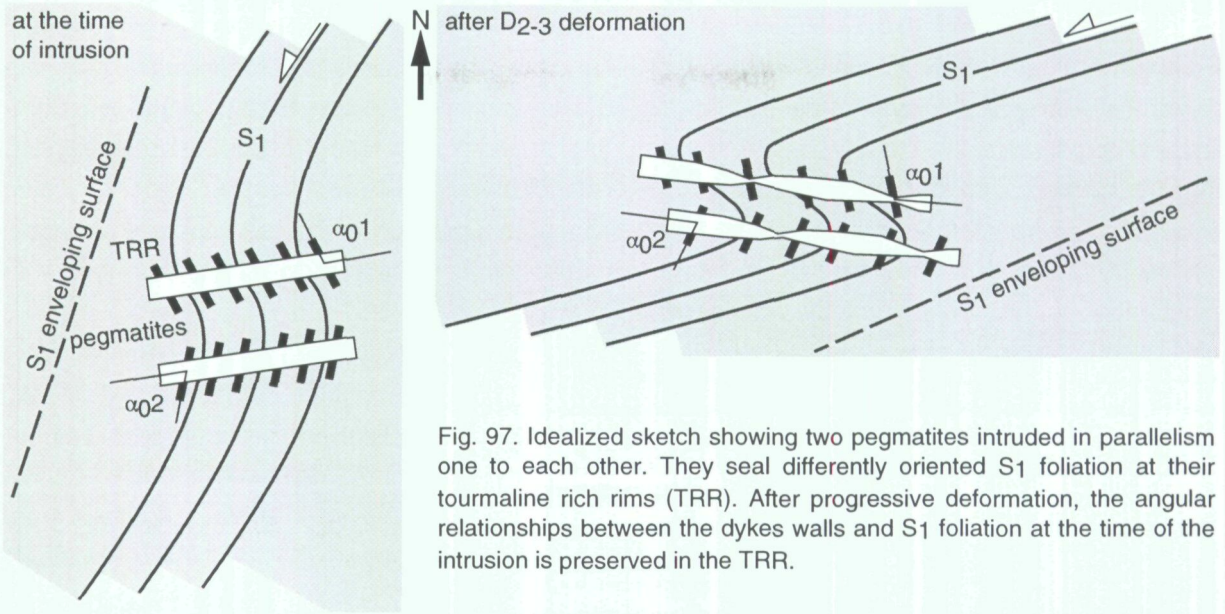

Fig. 97. Idealized sketch showing two pegmatites intruded in parallelism one to each other. They seal differently oriented S_1 foliation at their tourmaline rich rims (TRR). After progressive deformation, the angular relationships between the dykes walls and S_1 foliation at the time of the intrusion is preserved in the TRR.

Fig. 98. Sub-horizontal view of a thin pegmatite vein intruding parallel to the axial plane of a "S" shaped fold, while developing a tourmaline rich rim structure. Other veins in the photograph are sub-parallel to the S_1 foliation (lighthouse zone).

6.2. THREE-DIMENSIONAL ANALYSIS

After the above performed strain and kinematic analysis in horizontal sections, a three-dimensional model which tries to compatibilize all the observations will be now presented.

Before that, some more available information obtained from subvertical sections will be exposed. As already shown, asymmetric structures are better marked in flat-lying or gently dipping outcrop-sections than in steeper faces. This is consistent with a steeply dipping rotation axis (i.e. vorticity vector). Such rotation axis would therefore be closely parallel to the axes of the minor folds and the large cylindrical sigmoid, as well as it would be close in orientation to the subvertical stretching lineation. Actually, few asymmetric structures have been observed in steep surfaces. However, when observed, "northern block down" sense of shear in the vertical section seems dominant (Fig. 99).

Fig. 99. Vertical view of andalusite porphyroblasts rotated with respect to the $S_S/_1$ foliation. (Cala Portaló, north to the right of the photograph). The observed asymmetries indicate "northern block down" sense of shear.

A sinistral component of internal deformation in horizontal view and a N-down shearing component in sub-vertical sections are evident from rotated boudins and porphyroblasts.

This dip-slip shearing cannot be established using quartz c-axis fabric from a L-S tectonite from a high strain zone (Fig. 100). It is likely that strong static recrystallization effaced the syntectonic quartz fabrics, on the other hand well-defined in the mylonitized samples (Carreras et al. 1977, García 1983). Thus, although quartz c-axis fabrics did not provide additional kinematic information, it shows that the high strain zone is not a superimposed effect of later deformation, but a high temperature deformation zone.

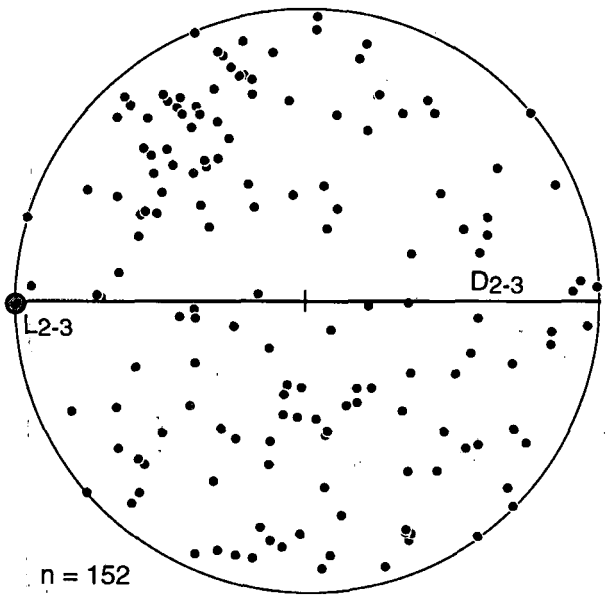

Fig. 100. Very weak preferred orientation of quartz c-axis of a L-S tectonite from a D_2 + D_{2-3} high strain domain (Tudela zone). The weak fabric cannot be used as a kinematic indicator.

The following approach model (Fig. 101) has been constructed considering the most relevant observations and deductions on strain and kinematics related to high temperature deformation. It is mainly referred to the north-eastern area, from where most data have been collected. The model presented in Fig. 101 is considered as the most compatible with the available data. Although analogue modelling was not available, a plasticine layered model was assembled in order to obtain a better understanding of the three-dimensional structure. The resulting three-dimensional geometry is shown from two different standpoints in order to get a complete illustration of the angular relationships between kinematic and structural elements. The main inferences from these sketches can be expressed in the following points:

1. The bulk structure approaches a heterogeneous vertical flexural flow affecting the previous $S_{S/1}$ anisotropy. The southern face of the body remains undeformed. In order to visualize layer-parallel shear components, a flexural slip has been represented instead of flexural flow. Also for the sake of simplicity, no minor folds resulting from layer shortening have been drawn.

2. The displacement vector is sub-parallel to the stretching lineation, being the bulk effect a translation of the northernmost blocks south-eastwards and predominantly upwards. Deformation is therefore consistent with a transpressional regime.

3. The sigmoidal shape of the S_1 foliation is controlled by the initial vertical attitude of this foliation and also by the sub-vertical position of the displacement vector. In this situation, the sigmoid axis and fold axes nucleate at a low angle to the stretching lineation. This fact is analogous to some shear zones in foliated rocks where the deflection axis is closely parallel with the stretching lineation (Carreras 1997).

4. Flexural flow involves layer (S_1)-parallel shearing, with a sinistral component in plane view and a N-down normal component in steep surfaces (green arrows in Fig. 101). On the other hand, the bulk flexure induces a bulk dextral rotation in plane view and N-up reverse motion (point 2). Contradiction between shear sense and displacements are only apparent, because both are geometrically consistent. Hence, in this case, kinematic sense of shear indicators do not indicate the sense of displacement and cannot be correlated with a given tectonic regime.

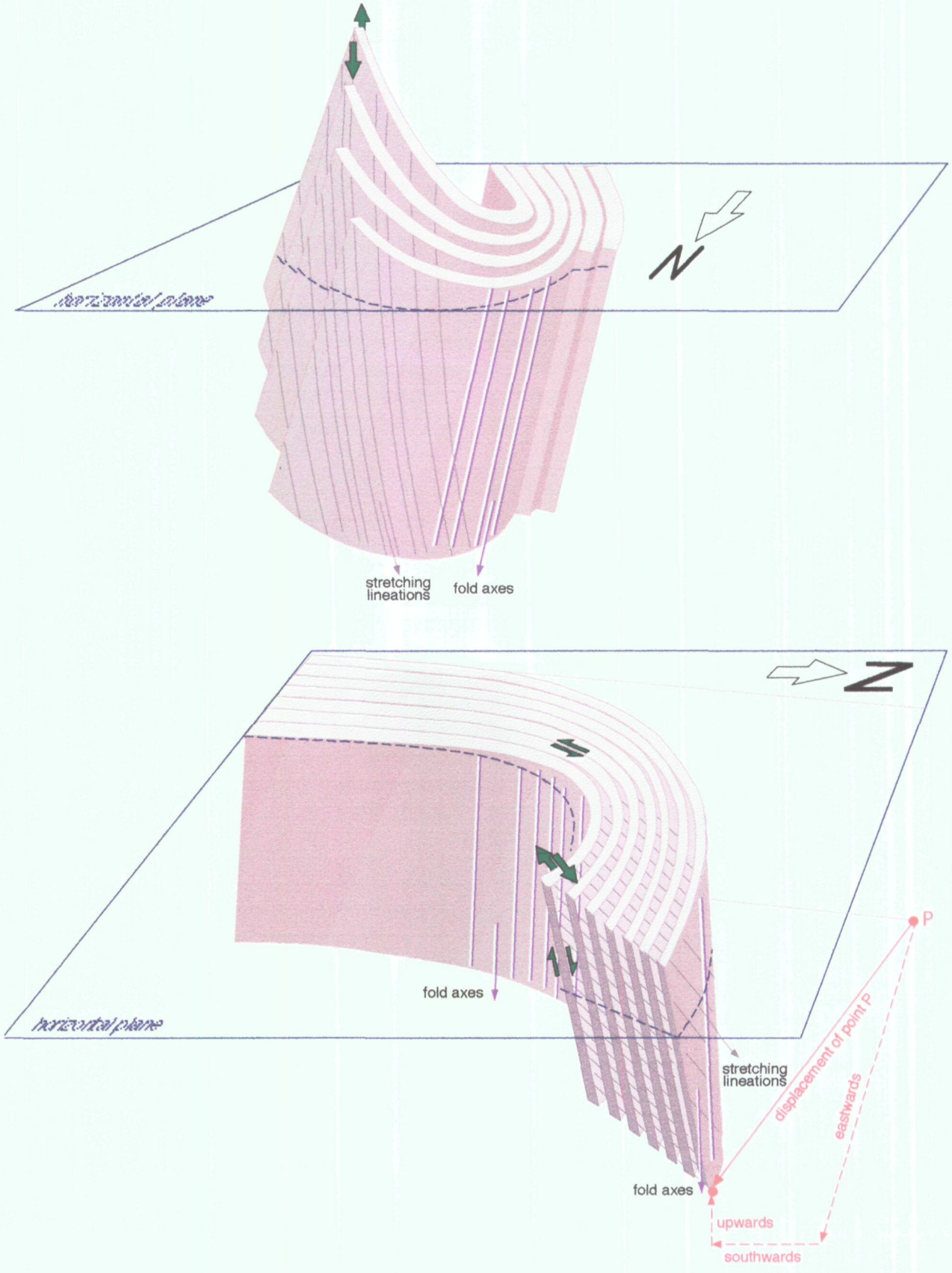

Fig. 101. Schematic block-diagrams which illustrate, from two different standpoints, the geometry and kinematics involved in the development of the high temperature structures (modelled for the north-eastern part of the study area). Green arrows represent the kinematic frame. Displacement undergone by a given point (P) is shown with red arrows. See text for detailed explanation.

Pegmatite dykes and, by extent, small bodies of granitoid emplaced syntectonically along gashes, controlled by the incremental strain ellipsoid and the mechanical anisotropy. A special attention has been paid to the E-W trending dykes, since they are the most frequent (Fig. 75, section 5.3), and because two-dimensional strain determinations reveal that such dykes might had undergone small amounts of rotation since their emplacement. It follows that these dykes were emplaced at relative small angles to the axial planes of folds and crenulation foliation. This trend corresponds to possible tensional or opening shear fractures, considering the space disposition of the instantaneous strain ellipsoid. In Fig. 102 a rough field comprising the orientation of different compatible R and T fractures has been plotted, together with the field comprising the variable orientations of the crenulation cleavage.

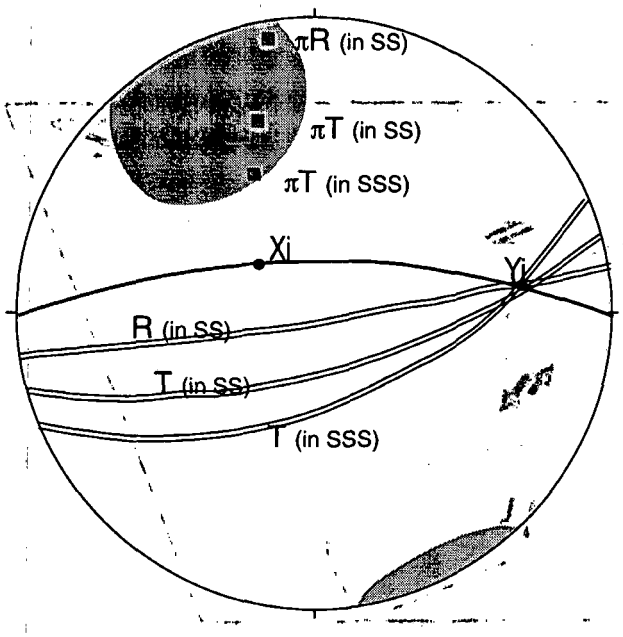

Fig. 102. Stereoplot showing the likely orientation of dykes emplaced along opening fractures developed by simple (SS) or sub-simple shear (SSS) in the high strain zones. For a given XiYi plane (corresponding to an strain increment), tensional fractures would plot in T. Opening Riedel shears formed by SS would plot as great circle R. Taking into account different possible orientations of XiYi ranging from E-W to WSW-ENE, the poles of opening fractures will fall in the grey area. Note that these dykes have predominantly WSW-ENE trend and steep south dips. Compare with Fig. 75. In this approach, no layer-parallel dykes have been plotted. In addition, the orientation of all these dykes would change slightly after emplacement, as a result of rotation towards the flow plane.

The proposed sequence of progressive events is shown schematically in Fig. 103a (plane view) and b (block-diagram). Sketches have been drawn assuming area loss in plane view (according to strain determinations in section 6.1.4) for isochoric (no instantaneous volume change) flow. Stage I represents the pre-D_2 initial stage, mainly characterized by the presence of a pervasive NNW-SSE trending subvertical $S_{S/1}$ foliation. At stage II, D_2 structures are developed (F_2 folds and S_2 crenulation cleavages) due to homogeneous sub-simple shear. $S_{S/1}$ parallel shearing and bulk flexure (depicting a dextral rotation of about 25° and vertical extension) are also displayed at this stage. Gashes are able to develop at certain orientations, controlled by the incremental strain ellipsoid and the mechanical anisotropy ($S_{S/1}$). At stage III, pegmatites intrude along these gashes while deformation continues. Dykes are subsequently strained and folds are further developed, together with a S_{2-3} foliation. Stage IV represents internal deformation and bulk rotation recorded by the schists, and D_{2-3} finite strains recorded by the pegmatite dykes at the end of D_{2-3} stage. Since strain gradients produce high and low strain domains, each individual stage can also be considered as representing finite deformations recorded at different domains. In this way, stage I could represent finite strain in low strain domains, and stage IV finite strains in high strain domains.

The space-time deformational history of a single initially cube-shaped volume of rock (schists bearing $S_{S/1}$ anisotropy) has been represented in Fig. 103c. In this case, the volume of rock is considered to be deformed homogeneously, recording high strains. The three sketches reflect how, during progressive deformation, the cube-shaped block is translated towards relative upper levels and to the south-east, while it is strained into a vertically-elongated parallelepiped.

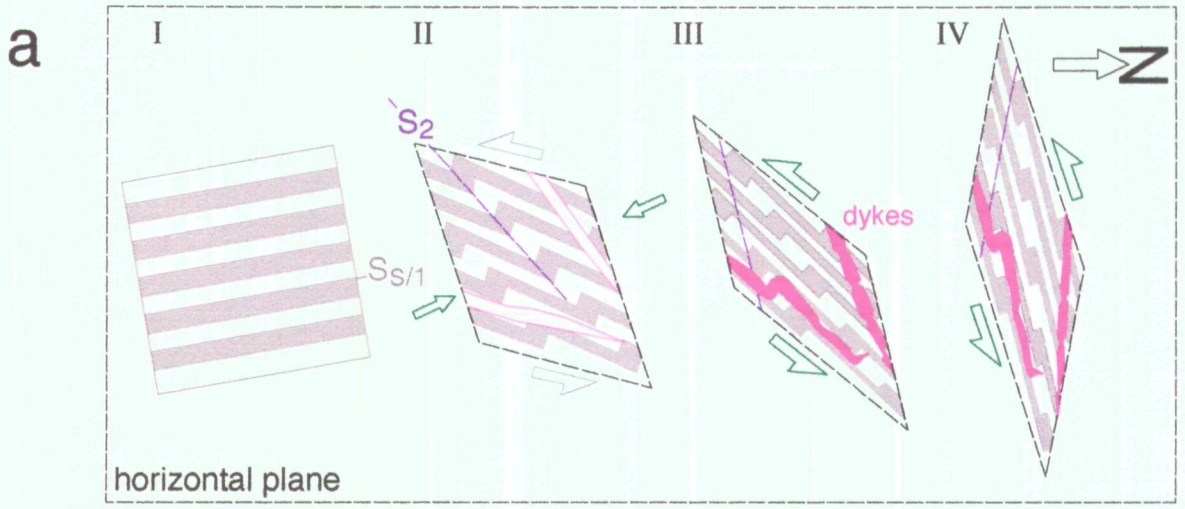

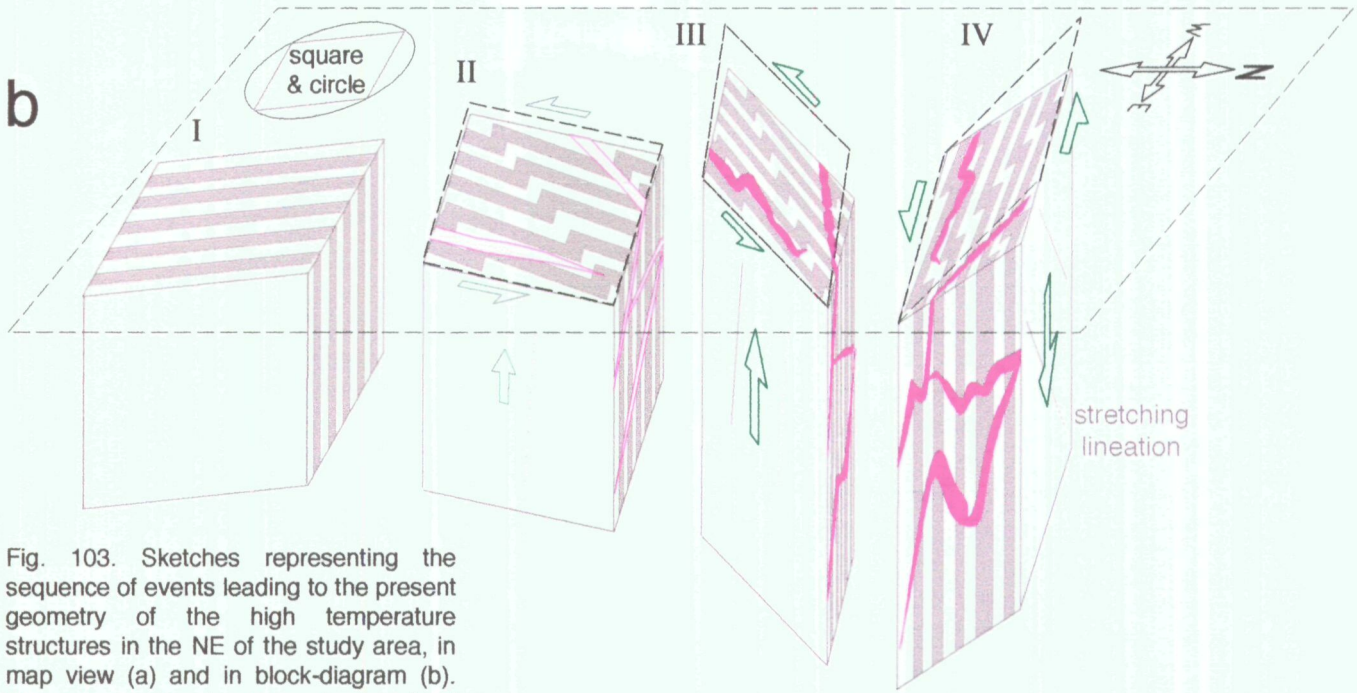

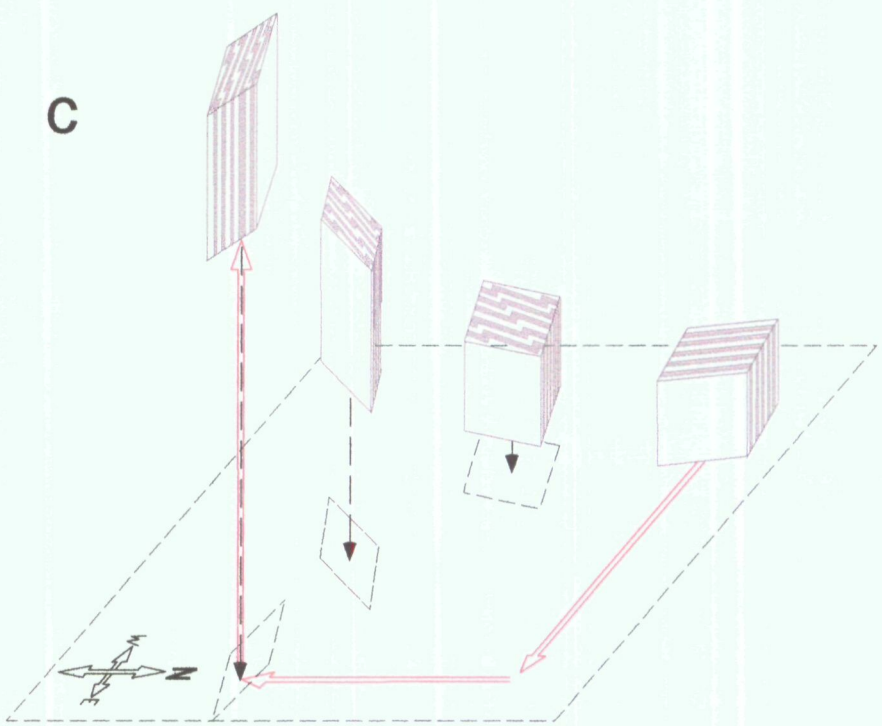

Fig. 103. Sketches representing the sequence of events leading to the present geometry of the high temperature structures in the NE of the study area, in map view (a) and in block-diagram (b). Stage I: pre D_2-structure, characterized by the presence of a sub-vertical $S_{S/1}$ schistosity. Stage II: bulk transpression (dextral shearing in the horizontal plane) causes clockwise rotation of $S_{S/1}$ and sinistral layer-parallel shearing (flexural flow), plus shortening in the horizontal plane and vertical extension. The S_2 crenulation cleavage and open fractures start to form at this stage. Green arrows represent the kinematic frame. Stage III: Pegmatites intrude along tension gashes or along surfaces of $S_{S/1}$. Continued deformation leads to strain of pegmatites and further development of crenulation cleavage ($S_{2\text{-}3}$). Stage IV: Further deformation produces high strain zones.
(c): Sketches showing the space-time deformational history of an initial cube-shaped volume of rock undergoing high strain deformation. Red arrows indicate the components of the finite displacement vector; black arrows indicate projections of each parallelepiped in an horizontal plane.

7 DISCUSSION AND CONCLUSIONS

7.1. REGIONAL ASPECTS

On the Cap de Creus geology

Polyphasic structures in the NE Cap de Creus peninsula are interpreted as part of a progressive deformational history. A continuity of events from prograde to retrograde metamorphic conditions is evidenced. Metamorphism started to develop high gradients at the time that deformation also displayed high strain gradients. Intensification of deformation and metamorphism coincides in space and time with magmatism (Fig. 104). The observed relationships between deformation, magmatism and metamorphism provide evidence that all three processes operated simultaneously in this segment of the Hercynian belt.

Tectonics involved non-coaxial progressive heterogeneous deformation and led to a complex mosaic of different patterns. Each tectonic event is inhomogeneous in space and characterized by non-coaxial deformation. In this way, orientation and style of structures change from one area to another, entailing the difficulty of correlation, even along a relative small zone. However, it has been possible to distinguish three main deformational events.

There is little evidence on the regional significance of the D_1 early deformation. However it seems that this early event was governed by tangential type tectonics, producing recumbent folds and/or thrusts with an associated gently dipping foliation. Although the original orientation of these structures could not be established, attitudes of intersection lineations point to a trend closer to N-S than to E-W. This tectonic event would be consistent with crustal thickening, involving a first metamorphic stage.

After the development of the S_1 pervasive foliation, regional deformation was characterized by the generation of steep structures. This is first manifested by a half-dome shaped macrostructure and possibly by the coeval onset of the thermal regional metamorphism. The trend of the domal structure is close to N-S.

D_2 and D_{2-3} non-coaxial progressive deformation gave rise to the development of upright folds. This folding event took place at prograde metamorphic conditions up to the peak of metamorphism. As a result of inhomogeneous deformation, a first structural zonation arose, evidenced by the presence of domains of low and high D_2 to D_{2-3} strain. A NE-SW to E-W trending subvertical transposition foliation was created in the high strain domains. High strain zones, mostly developed in the north, could represent the stretched and sheared limb of a large vertical fold. Strain and kinematic analysis of these structures reveals that deformation took place in a broadly transpressive regime involving vertical extension and NNW-SSE subhorizontal bulk shortening. Reverse motions, with a minor dextral component, were prevalent at these stages. Deformation was accompanied by syntectonic emplacement of small bodies of granitoids, corresponding to a calc-alkaline sequence, and a swarm of anatectic pegmatite dykes. A sequence of intrusions from the most basic to the acid types is established on the basis of overprinting relationships and intensity of deformation recorded by each magmatic type, being all syntectonic with respect to progressive D_2 to D_{2-3} deformation.

The interaction between deformation, plutonism and metamorphism ("tectonoplutonometamorphism") would explain the high thermal gradients observed in the study area (Fig. 104). The rocks now located in the north would have experienced a temperature rise due to the vicinity of hot, deep-level material. Magmas would have risen towards upper levels and along high strain domains, possibly favoured by vertical extension. Zones of isometamorphism became rather steep and thin towards de core of the subvertical "high strain intrusion zone", and even the anatectic limit could have been superimposed over lower grade zones, in analogy with the model known as the telescopic effect (den Tex 1963). As deformation proceeded, just after the peak of metamorphism (when pegmatites intruded), an horizontal shortening greater than 50% in domains of intense deformation might account also for narrowing isometamorphic zones.

Deformation proceeded with heterogeneous development of D_3 folds and shear zones in post-magmatic and retrograde conditions, leading to the superimposition of structural and metamorphic zonations. The overall tectonic evolution from D_2 to D_3 is characterized by (i) a clockwise rotation of structures, from upright NE-SW to NW-SE with southern vergence; (ii) a broadly transpressive regional regime, starting with a contraction or pure shear-dominated transpression and later evolving to

wrench-dominated transpression, and (iii) progressive strain localization along narrow transposition bands and shear zones (mylonite belt) at low temperature conditions. Therefore, the overall Hercynian tectonometamorphic evolution involved a sequence of events which are difficult to separate in distinct phases. In consequence, the late folds, together with the shear zones are interpreted to be Hercynian. Thus, any assumption assigning Alpine ages would also consider the high temperature structures (D_2 to D_{2-3}) Alpine in age. This would be in contradiction with the geology of the NE Iberian Peninsula, where there is abundant evidence of post-Hercynian sedimentary rocks unconformably covering late folds and metamorphic and igneous rocks.

In consequence, the effect of Alpine structural overprinting is local and restorable. In the Cap de Creus peninsula, the large E-W trending doming structure which separates a northern and a southern domain, where Hercynian structures dip to the north and to the south respectively (I.T.G.E. 1994a) could be in part Alpine, and would have been responsible for the overturning of the southern border. This overturning has analogies to Alpine structures along the southern border of the Pyrenean Axial Zone (i.e. Nogueres zone).

Comparison with adjoining areas

The adjacent Roses and Rodes granodiorite massifs, although separated from the migmatite domains, are likely connected to the proposed magmatic and tectonometamorphic evolution recorded in the northern part of the Cap de Creus peninsula. Spatial association of migmatite domains and deepest parts of stratoid batholiths is common in the Hercynian of the Pyrenees (e.g. Albera, Roc de Frausa and easternmost Andorra-Mont-Lluis massif). Furthermore, these batholiths, mainly emplaced in shallow levels (Fig. 104), recorded structural features which have been interpreted as a result of progressive deformation during cooling (Simpson et al. 1982; Gleizes 1992, Carreras et al. in review). Synmagmatic fabrics in the granodiorites can be correlated with D_2 and D_{2-3} structures in the study area, and late granodiorite shearing with D_3 folds and shear zones. Taking into account the bulk structure of the Cap de Creus Peninsula and the geometry drawn for other eastern Pyrenean batholiths, it is conceivable that the Roses and Rodes granodiorites were linked to the migmatite domains but lying at a higher, now eroded, structural level.

In a broader regional setting, it is not an easy task to correlate the tectonic evolution recorded in different massifs of the Axial zone and of the North Pyrenean massifs. The most significant vertical structural zonation, consisting of an infrastructure in deep-seated levels and a suprastructure in shallow levels, described in the central Axial Zone (de Sitter & Zwart 1960, Oele 1966) and reviewed in Carreras & Capellà (1994) and García-Sansegundo (1996), is not manifest in the easternmost Axial Zone. Neither are the common domal structures recognized in the Hospitalet- Aston, Canigó-Carançà, Roc de Frausa gneissic domes, or in the Garona-Bossost metasedimentary dome. As a consequence, the correlation problem between the Cap de Creus structure and other massifs awaits solution. However, a general outline will be proposed.

D_1 early structures in the Cap de Creus peninsula (S_1 foliation) might be correlated with the main foliation or schistosity, formed originally with a gently dipping or flat-lying attitude, which characterizes the infrastructure in the gneissic domes (e.g. the Canigó and Aston massifs, Garona dome). On the other hand, D_2 to D_3 progressive folding in the Cap de Creus seems to share analogies with upright folds which affect inhomogeneously the flat-lying schistosity in the infrastructure. The composite S_{1-2} flat-lying foliation, recognized in the infrastructure (e.g. Santanach 1973, Casas 1978) has not been recognized in the Cap de Creus, while steep S_2 foliations prevalent in the Cap de Creus appear less manifest in other massifs. Whether flat-lying S_2 (e.g. in the Canigó or in the Bossost area) and steep S_2 (in the Cap de Creus) are contemporaneous or not is a key question which will require further detailed structural analysis. A preliminary answer could be obtained by comparison with the nearby Roc de Frausa massif.